PHYS3051 Lab Report 1
Antenna Radiation Patterns

Ryan White
s4499039
with partners Sascha Lawton, Ceri Harris

Semester 1, 2023

Abstract

Herein we discuss the utility of using specific length dipole antennae to receive signal from a microwave source. We find that dipole antenna lengths of half-integer multiples of the wavelength yield the most consistent radiation patterns as determined by their calculated directivity and half-power beam width values, where a dipole antenna length of $\lambda/2$ is characterised by the most consistent pattern in the sample size tested. We observe values for these parameters typically outside of 1σ from theoretical values which are derived from idealised assumptions. The experimental setup involved observing approximately uniform microwave radiation across a dipole antenna as the dipole antenna rotated about a full rotation with respect to the light source. We identify limitations in our experimental setup, and qualitatively draw conclusions on the effects of these limitations in relation to the observed discrepancy from theory. Suggestions are made to minimise (and in some cases avoid) these systematic errors in future investigations.

1 Introduction

Antennae are physically simple probes into a complex world of physics. These simple lengths of conducting metal, situated in just the right orientation within electrical circuits, lay the foundation on which modern communications are built. In fact, the submission of this very report over the internet is made possible by the physics discussed here.

With such an integral place within modern life, understanding the intricacies of antennae is of the utmost importance. Herein we investigate the variability of an induced electric signal via a dipole antenna under certain variable conditions, with an approximately planar microwave-spectrum source being at the center of analysis.

2 Theory

We begin by directing discussion towards the utility of the dipole antenna. Constructed as two conducting metal cylinders, separated by a small gap between their bottom faces, dipole antennae form a relatively simple induced radiation pattern that aligns well with established theory. The theory in question, however, is subject to numerous idealised approximations that are not physically testable. In particular, two of the more extensive approximations are those that necessitate that the 'width' of the antenna (that is, the radius of its cylinder) is infinitesimally thin, and that the separation between the two dipole halves is also infinitesimally thin [3].

Upon making all of these idealised assumptions, though, we're able to calculate the predicted radiation pattern through the induced electric field via equation (1).

$$P_{\text{pred}}(\theta) - \frac{\cos(\frac{1}{2}kL\cos\theta) - \cos(\frac{1}{2}kL)}{\sin\theta} \tag{1}$$

Directivity is defined as the ratio of the maximum power (in the main lobe of the radiation pattern) to the average power over the angular space [1]. As directivity approaches order unity, we can infer that the radiation pattern is more uniform (in the general case) and so is more consistent over a change in angle. For an antenna at a constant polar orientation with respect to a wave source, we can calculate the directivity (using the same idealised approximations as before) as in equation (2).

$$\begin{aligned} D &= 2\left(\int_0^{\pi} |P(\theta)|^2 \ \sin\theta \ d\theta\right)^{-1} \\ &= 4\left(\int_0^{2\pi} |P(\theta)|^2 \ |\sin\theta| \ d\theta\right)^{-1} \end{aligned} \tag{2}$$

Of course, directivity may approach order unity for a range of radiation patterns, even for those with several pronounced lobes and chaotic behaviour. To fully assess the consistency in the induced signal of an antenna, we also calculate the *half-power beam width* which is defined as twice the change in angle required for the power in the largest lobe (in the radiation pattern) to drop to half of its maximal value. While no *simple* analytic

formula exists to calculate this (as is for the case with directivity), we can calculate the half-power beam width using simple coding techniques on existing data. Algorithm 1 shows a linear search technique that begins at the maximum power value and progressively iterates over the angular measurements, comparing power values at each step. We note that this algorithm can be applied

Algorithm 1 Finding the Half-Power Beamwidth, θ_{HP}

$\theta_{\max} \leftarrow \theta$ such that $|P(\theta)| = \max|P|$
$\theta_i \leftarrow \theta_{\max}$
while $|P(\theta_{\max})| - 3 < |P(\theta_i)|$ **do**
  $\theta_i \leftarrow \theta_i + \Delta\theta$
end while
$\theta_{\text{HP}} \leftarrow 2|\theta_{\max} - \theta_i|$

to the predicted radiation pattern (1) (on an arbitrarily precise angular domain) to obtain theoretical values for the half-power beam width. Similarly, the predicted radiation pattern can be used to infer theoretical values of the directivity.

For an antenna with a low value of directivity and a large half-power beam width, we can conclude that it will have a consistent signal for a large range of angular values. Antennae that are characterised by this are attractive for a large number of real-world applications, as they can receive information in almost any orientation with respect to the source.

As mentioned previously, there are numerous idealised approximations made to link the observations to theoretical predictions. Another of these, for which all of the observations fundamentally rely on, is the *far field approximation*. The far field approximation is a distance such that *"the angular distribution of radiation is independent of the distance r."* [2]. Although in actuality this condition is never perfectly satisfied, we may nevertheless calculate the distance for which this condition is valid via

$$r_{\text{ff}} \geq \frac{2(L_{\text{source}} + L_{\text{test}})^2}{\lambda} \tag{3}$$

In this equation [3], both the length of the source antenna (see Section 3 for the experimental setup) and the dipole test antenna affect the far field separation, and so provides a more conservative estimate compared to [2].

3 Experiment

To analyse the radiation pattern in our dipole antenna, we used a microwave source that emitted light with wavelength $\lambda = 0.032$m. As Figure 1 shows, the makeup of the microwave source was composed of a Gunn Diode, Isolator, Pin Modulator and a horn antenna. Here, the horn antenna ensures that the radiation being emitted in the direction of the dipole antenna is polarised in the same orientation as the dipole (and so a radiation *pattern* may be observed as the polarisation vector changes relative to the dipole). Directly in front of the open face of the horn is the dipole antenna fixed onto a rotating platform. Care was taken to ensure that both the microwave source was pointing directly at the test antenna, and that the central height of the horn open face aligned with the test antenna. For the duration of rotation of the antenna, a value of $\Delta\theta = 0.5^{\text{o}}$ was chosen for the angular increments on the rotating antenna platform. This value was chosen compared to a larger step value to constrain uncertainties in values of the half-power beam width (and to a lesser extent, the other quantities of interest). Conversely, we chose this value compared to a smaller step value to make for a more time-efficient data collection process.

The test dipole antennae were situated directly in front of the horn antenna as in Figure 1. In the diagram, we'd varied the distance d between the horn and dipole as an independent variable across experimentation. For each data collection, the radiation pattern at a single distance separation was taken before moving onto the next data collection. For each distance separation, we also observed the radiation pattern across 3 key dipole antenna lengths: $\lambda/2$, $3\lambda/2$, and 4λ. Although more antenna extensions were available to us, we chose those specific lengths both to reduce experimentation time and also to encapsulate a broad spectrum of radiation patterns on account of the varying lengths.

To help reduce interference on the antenna from any background radiation, anechoic mats were situated around and above the test antenna and rotating table. The placement of the mats effectively formed a concave structure around the test antenna which shielded it from the majority of the lines-of-sight to the antenna. Furthermore, we placed anechoic mats on the surface of the table between the source and test antennae to minimise the reflection from the flat, smooth table.

3.1 Method

Once the experimental apparatus was setup as in Figure 1 and the experiment description, we connected the antenna and rotating table to the PC with the `CASSY Lab 2` program open. Beginning with a distance of $d = 1.8$m between the dipole and the source antenna, we set the `CASSY` program to record `Level A, a,` θ, and `U`. We then set the program to rotate the platform in increments of $\Delta\theta = 0.5^{\text{o}}$, recording the magnitude of radiation across the 360^{o} angular domain. This data collection was repeated 3 times, and then the antenna extensions were screwed into the ends of each dipole half so that the dipole had a length of $3\lambda/2$. This triple collection

was then repeated, and finally the extensions were replaced with those that make the dipole have a length of 4λ. Upon each data collection, a `.csv` file of the data was saved to the PC with an identifying filename corresponding to the variable parameters. This process (collection for each iteration and antenna length) was then repeated for distances of $d \in [0.75, 1.3]$ meters.

4 Results

The radiation pattern data collected over the experiment is displayed the polar plots of Figures 2 and 3. All data analysis and plotting was contained within a Python script, where we utilised `matplotlib`, `numpy`, and `scipy` for the bulk of analysis. Tabulated values of the calculated directivity and half-power beam widths are shown in Table 1.

Antenna Length (λ)	Directivity	Half-Power Beam Width
1/2	1.597 ± 0.008 (1.641)	84.0 ± 17 (56)
3/2	2.063 ± 0.059 (2.224)	44.0 ± 5.6 (28)
4	3.611 ± 0.059 (3.541)	34.6 ± 3.8 (16)

Table 1 Calculated Directivity and Half-Power Beam Widths for each antenna length. Gaussian uncertainties were assumed in each case, with the uncertainties in half-power beam width calculated via the standard deviation across all observed samples. Uncertainties in directivity were calculated via Monte Carlo uncertainty propagation on the numerical integration, with data uncertainties given by that in Figure 2. Idealised (theoretical) values are given in parentheses for each cell, naturally without uncertainty.

We note that, with a horn antenna length of 0.05 ± 0.01m, the far field approximation holds for all tested distance values with the $\lambda/2$ length dipole antenna, the 1.3 and 1.8m distances for the $3\lambda/2$ dipole, and *none* of the distance values for the 4λ dipole. On comparing the plots within Figure 2 we see that the data aligns most with the theoretical values for the $\lambda/2$ and $3\lambda/2$ dipole antennae. The reduced chi-square statistic for each of the three data-model comparisons is $\chi^2_{\text{dof}} \simeq 2.66$ for the $\lambda/2$ antenna, $\chi^2_{\text{dof}} \simeq 1.37$ for the $3\lambda/2$ antenna, and $\chi^2_{\text{dof}} \simeq 24.35$ for the 4λ antenna. This range of chi-square values further shows the importance of satisfying the far field condition in comparison to theory, as the 4λ antenna (which didn't satisfy this approximation for *any* distance) was far out of agreement with the theoretical values. On inspection of the bottom plot in Figure 2, we see that while the number of nodes and peaks matches theoretical predictions, the angular positioning (and spacing) of these nodes is skewed likely as a result of this failure to meet the far field condition. With such a long antenna, rotation nearer to the $[\pi, 2\pi]$ angles (where the antenna is parallel with the incident wave vector) represents the largest delta separation between the two ends of the dipole antenna with respect to the microwave source; this is where the prediction breaks down and we see the effects of the far field approximation failing. This argument is supported by inspection of the bottom plot in Figure 3, where we see the angular position of the maxima lobes shifting towards the theoretical position as the distance between dipole and source increases.

We note that the discrepancy between theory and data for the $\lambda/2$ and $3\lambda/2$ dipole antennae must be due to other effects than the distance between source

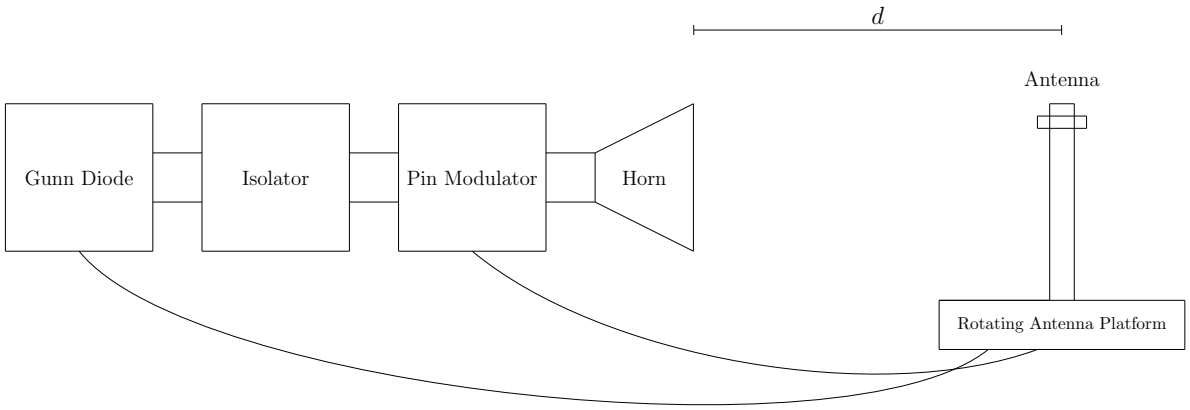

Figure. 1 Experimental setup to measure the radiation patterns. The distance we measured between the horn and the antenna is denoted by d in this diagram; this value remains constant as the antenna platform rotates with respect to the center of the antenna. The Gunn Diode and Pin Modulator were connected directly to the Rotating Antenna Platform via supplied cables, and the entire source was raised so that the center point of the horn aligned with the antenna (as opposed to the height of the source depicted in the diagram).

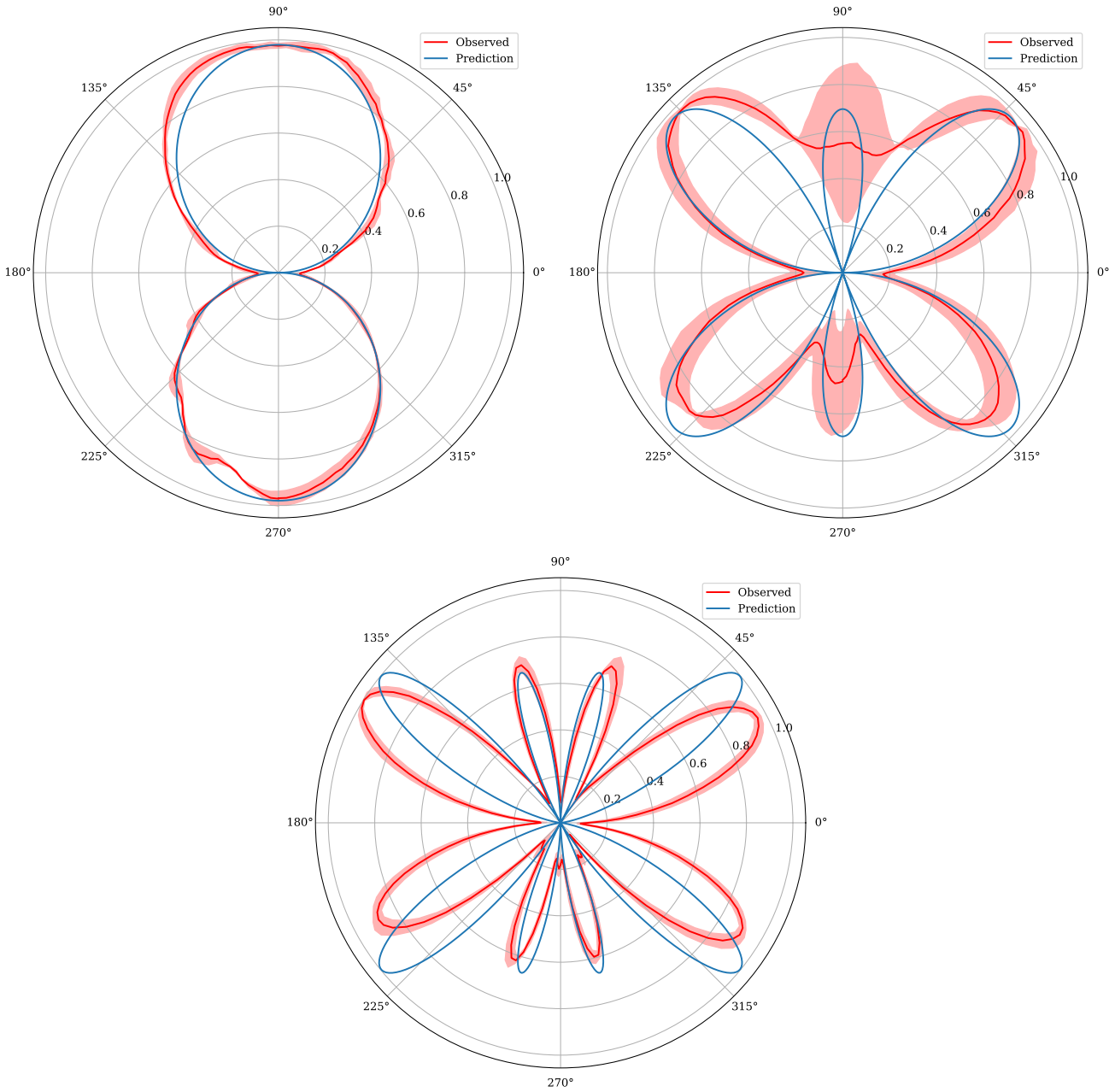

Figure. 2 Normalised observed and predicted radiation patterns for different length antennae. Radial values represent the magnitude of the electric field at the test antenna, and angular values represent the rotation angle of the antenna. *Top left:* radiation pattern for a $\lambda/2$ antenna length. The shaded region represents uncertainty in the observed values based off of the variance in multiple observations. Overlaid in blue is the prediction calculated by Eq. (1), using an idealised Maxwell equations. *Top right:* radiation pattern for a $3\lambda/2$ antenna length. *Bottom:* radiation pattern for a 4λ antenna length.

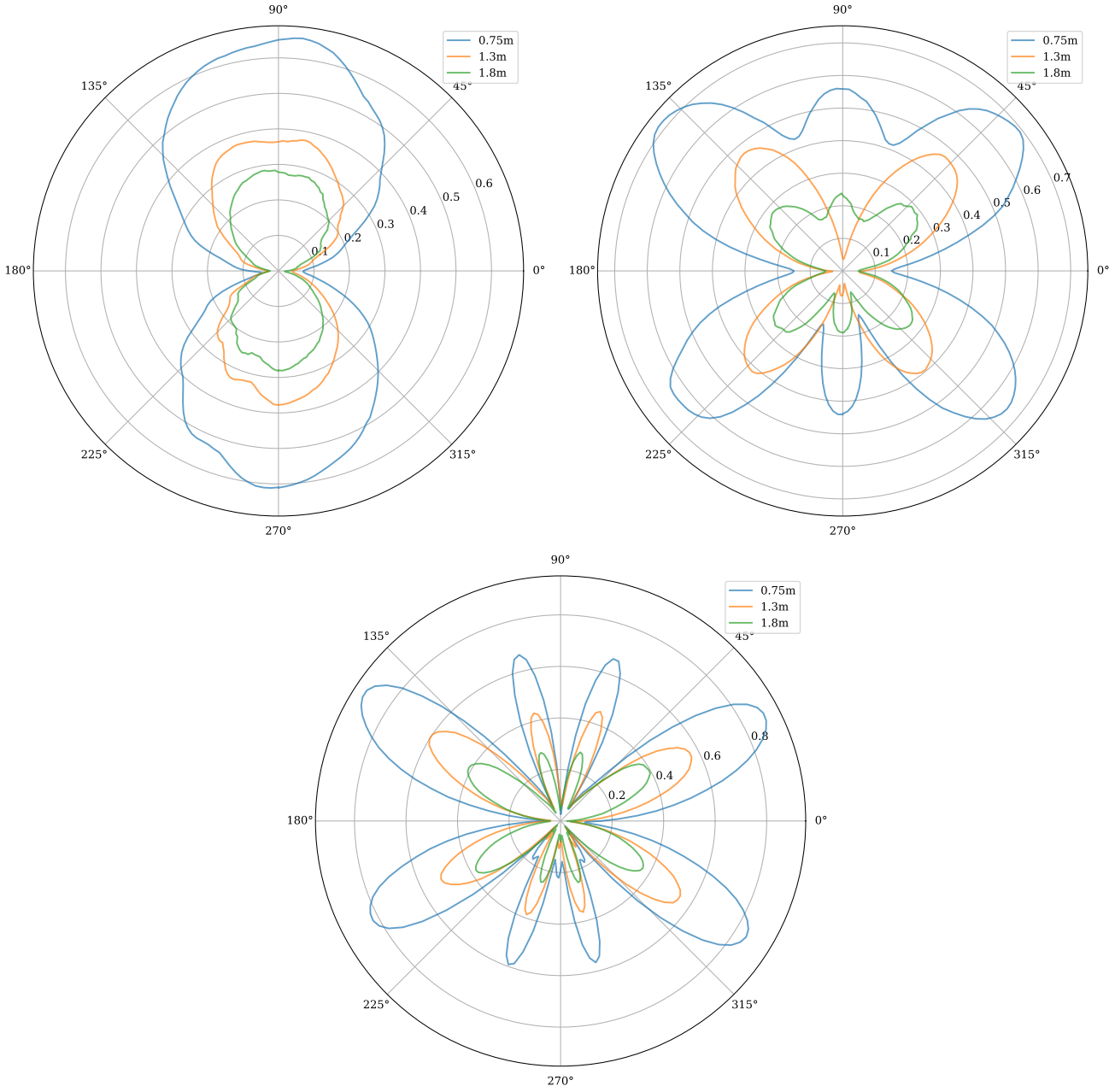

Figure. 3 Radiation patterns for each antenna length and distance observed. Each pattern is coloured according to the distance between the test antenna and the leading edge of the pyramidal horn antenna, where the uncertainty in this distance is approx ± 0.05m. Axis meanings are as in Figure 2. Radiation patterns of the $\lambda/2$, $3\lambda/2$, and 4λ test antenna lengths correspond to the top left, top right, and bottom plots respectively.

and dipole. Most notably for the $\lambda/2$ antenna is the approximation that the dipole is infinitesimally thin. The approximation holds for a length to radius ratio of the dipole antenna of above 60, where in reality this ratio was closer to $\sim$ 20 for the $\lambda/2$ dipole. This was likely the cause of the more oblate radiation pattern as opposed to the prolate lobes predicted by equation (1) as seen in Figure 2.

5 Discussion

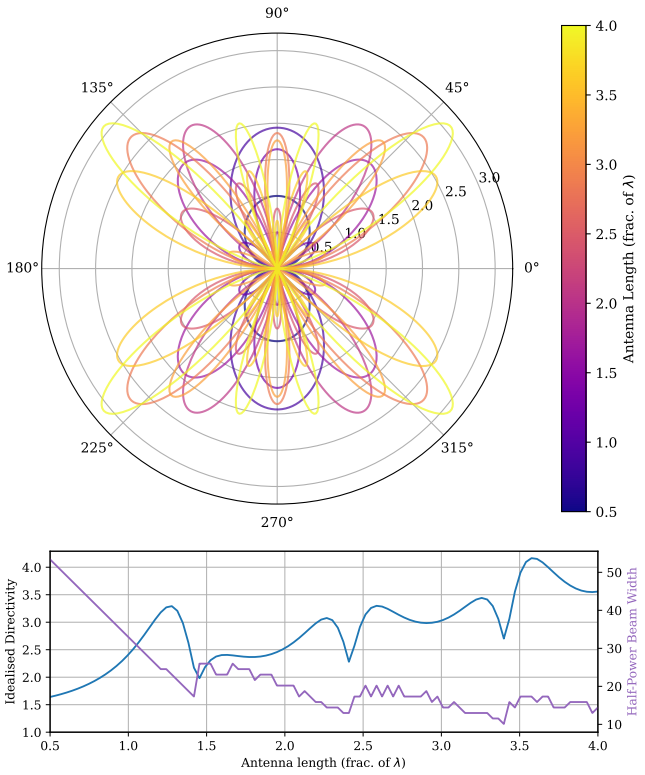

Figure. 4 *Top:* predicted radiation pattern for varying antenna length. 10 linearly spaced antenna lengths between $\lambda/2$ and 4λ were plotted, with the colour of the pattern corresponding to the antenna length. *Bottom:* Idealised directivity and HPBW based on the predicted radiation pattern for 10^2 antenna lengths in the range $[\lambda/2, 4\lambda]$.

Our investigation into the radiation pattern across different length antennae revealed why a particular geometry of antenna are predominately used in real applications. As the figures in the Results section show, a shorter antenna is characterised by a more consistent radiation pattern with fewer lobes and nodes and an average value that more closely aligns with its maximum value (i.e. a directivity resembling order unity). Figure 4 shows the predicted radiation pattern across a range of antenna lengths. Here we see that the case of $L = \lambda/2$ does correspond to the most uniform directivity in the relevant range of dipole lengths.

Although the radiation pattern is less uniform for larger antenna lengths, we note that the magnitude of the induced field in the main lobe is typically larger (keeping source-dipole separation constant) (Figure 3). On this note, we see in Figure 4 (bottom) that there exist local minima in the predicted directivity close to half-integer multiples of the incident wavelength. Simultaneously, we see approximate local *maxima* in the half-power beam width close to each directivity minimum, which again makes for an even more consistent induced field with respect to angle. This provides valuable insight into why $n\lambda/2$ antenna lengths are typically used, as for most applications, a more uniform source is desired.

Ultimately, systematic error was inferred within our experimental data. As mentioned previously, we note that the far field condition wasn't satisfied for *some* of the data collections, and was only just valid for other collections. In future analyses, we recommend that larger distances between the horn and test antennae be tested. Further, performing the experiment within a totally anechoic environment (as opposed to merely situating mats around the test antenna and along the floor parallel to the incident wave vector) may reduce variations in the radiation pattern from theory.

6 Conclusions

Using a dipole test antenna and microwave source experimental setup, we conclude that half-integer wavelength dipole antenna lengths are desired (in real-world applications) to ensure as consistent a signal as possible by minimising the directivity in the induced electric field, and maximising the half-power beam width. Our investigation was impacted by systematic errors as a result of failure to meet stringent far-field approximation conditions, and we make recommendations that may reduce these effects in future experiments.

References

[1] T.A. Milligan. *Modern Antenna Design*. McGraw-Hill, 1985. ISBN: 9780070423183. URL: `https://books.google.com.au/books?id=sxUoAQAAMAAJ`.

[2] S. J. Orfanidis. *Electromagnetic Waves and Antennas*. 2016. URL: `https://www.ece.rutgers.edu/%5C~orfanidi/ewa/`.

[3] PHYS3051. *Fields in Physics Laboratory – Antenna Experiment*. 2014.